ADVANCED ENERGY MATERIALS
www.advenergymat.de

Molecular Catalyst with Near 100% Selectivity for CO_2 Reduction in Acidic Electrolytes

*Zhan Jiang, Zisheng Zhang, Huan Li, Yirong Tang, Yubo Yuan, Jie Zao, Hongzhi Zheng, and Yongye Liang**

The electrocatalytic carbon dioxide reduction reaction (CO_2RR) in an acidic medium is conducive to the efficient utilization of CO_2 by preventing the formation of carbonate/bicarbonate. However, acidic media are more favorable for the hydrogen evolution reaction (HER), resulting in unsatisfactory CO_2RR selectivities. It is demonstrated that the molecularly dispersed electrocatalyst of β-tetra methoxy-substituted nickel phthalocyanine on carbon nanotubes (NiPc-OMe MDE) can efficiently catalyze CO_2RR in acidic media (pH 2 to 0.47) with Faradaic efficiencies of CO >98% over a wide range of current densities from −50 to −400 mA cm^{-2}. It is found that the superior selectivity performance can be attributed to the presence of potassium ions, the high preference of CO_2RR over HER on the active site, and few side reaction sites. The study illuminates the potential of molecular electrocatalysts for selective and rapid reduction of CO_2 in acid media.

1. Introduction

The electrocatalytic carbon dioxide reduction reaction (CO_2RR) provides an attractive route to produce chemicals while mitigating greenhouse gas emissions.[1–5] A two-step technology for CO_2RR is considered an economical strategy, where CO_2 steam is converted to CO in the first production unit and the produced CO can be efficiently reduced in the second unit to produce multi-carbon (C_{2+}) products such as ethylene and ethanol.[6–10] Compared with the direct CO_2RR, this two-step approach can allow CO reduction in an alkaline medium, not only facilitating the C—C coupling reaction for highly selective C_{2+} production, but also avoiding the reaction of CO_2 with alkaline electrolytes.[11] Therefore, efficient CO_2-to-CO conversion is important. Currently, the CO production process mainly operates in alkali or neutral media for high Faraday efficiency (FE).[12–16] However, CO_2 reacts with the electrolyte to form carbonate or bicarbonate in alkali or neutral media, leading to short-lived catalysis, electrolyte loss, and substantial CO_2 loss (>50%).[17,18] The carbonate or bicarbonate formation in CO_2RR significantly increases the operating costs and severely limits its prospects.[11]

CO_2RR in acidic media can eliminate carbonate or bicarbonate formation and thus facilitate efficient CO_2 utilization.[19–26] However, it is challenging to achieve high FE(CO) in acidic CO_2RR because the acidic environment is kinetically more favorable for the hydrogen evolution reaction (HER) than CO_2RR.[19–22] Thus, common CO production catalysts generally show much lower selectivity in strong acids. Recently, it was reported that K^+ in the electrolyte can shield the electrode electric field and inhibit the transport of hydrogen ions, thus inhibiting HER.[19] With K^+, the rapid consumption of surface hydrogen ions at large current densities can increase the pH near active sites, enabling efficient electrocatalytic CO_2RR.[23,26] Several electrocatalysts, such as Au,[19,22] Ag,[21] and Ni_5@NCN,[20] have shown the ability to eletrocatalyze CO_2RR into CO in acid, but their FE(CO)s were often below 90% and high CO selectivity could only be achieved in a narrow range of current densities.

Molecular electrocatalysts with well-defined structures can allow precise construction of active sites, affording excellent catalytic selectivity in many reactions, such as CO_2RR and the O_2 reduction reaction.[27–29] Recently, it was reported that Ni cyclam complexes can perform acidic CO_2 reduction in bipolar membrane gas diffusion electrodes, but the CO partial current density is lower than −34 mA cm^{-2}, and FE(CO)s were lower than 63%.[30] Electrocatalytic CO_2RR in an acidic medium is still challenging for molecular electrocatalysts that can work with high selectivity, larger current density, and long-term stability.

Herein, we report that nickel phthalocyanine electrocatalysts can selectively produce CO for CO_2RR in acidic media (**Figure 1**a,b). The molecularly dispersed electrocatalyst (MDE) formed by anchoring β-tetra methoxy-substituted nickel phthalocyanine (NiPc-OMe) molecules on carbon nanotubes (CNTs) demonstrates excellent selectivity with FE(CO) >99% over a wide range of current densities from −20 to −400 mA cm^{-2} in

Z. Jiang, Z. Zhang, H. Li, Y. Tang, Y. Yuan, J. Zao, H. Zheng, Y. Liang
Department of Materials Science and Engineering
Southern University of Science and Technology
Shenzhen 518055, China
E-mail: liang.yy@sustc.edu.cn
Z. Zhang
Department of Chemistry and Biochemistry
University of California
Los Angeles, CA 90095, United States
Y. Liang
Guangdong-Hong Kong-Macao Joint Laboratory for Photonic-Thermal-Electrical Energy Materials and Devices
Southern University of Science and Technology
Shenzhen 518055, China
The ORCID identification number(s) for the author(s) of this article can be found under https://doi.org/10.1002/aenm.202203603.

DOI: 10.1002/aenm.202203603

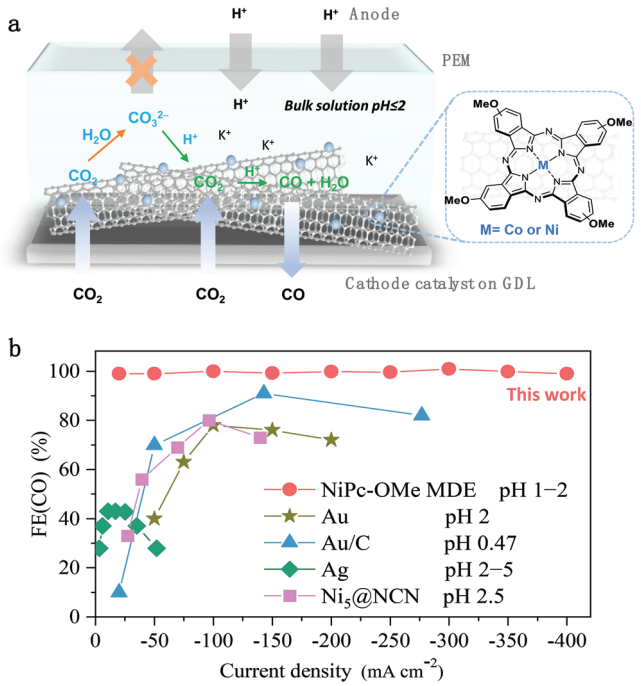

Figure 1. Electrochemical CO_2RR in acid. a) Schematic of CO_2RR catalyzed by metal phthalocyanine MDEs; (b) FE(CO) comparison of NiPc-OMe MDE and the reported Au,[22] Au/C,[19] Ag,[21] and Ni_5@NCN[20] at varied current densities.

the pH 2 electrolyte. Even in strongly acidic media (pH ≤ 1), NiPc-OMe MDE can still maintain high selectivity and work stably at high current densities. It is found that the presence of K^+ is necessary to suppress HER. A comparative study of CoPc-OMe MDE shows lower CO selectivities, especially under high current densities, illustrating the advantage of NiPc-OMe MDE with a lower preference for HER. Another control, a nickel single-atom catalyst (Ni-SAC) synthesized by high-temperature pyrolysis is unable to maintain high selectivity in strong acidic CO_2RR possibly due to its complex active site structures.

2. Result and Discussion

2.1. Preparation of the NiPc-OMe MDE Electrode

We first synthesized NiPc-OMe molecules and anchored them on the surface of multiwalled CNTs via π-π interaction by sonication in an *N*, *N*-dimethylformamide (DMF) dispersion, affording NiPc-OMe MDE based on our previous method (see details in Supporting Information).[12] NiPc-based catalysts have shown high selectivity of CO production for CO_2RR in neutral electrolytes and electron-donating substituents (such as -OMe) can improve the structural stability of MPc molecules in CO_2RR.[12,31] It should be noted that MPcs were less studied in acid CO_2RR and they showed low FE(CO) of below 50%.[32] The hybridization between NiPc-OMe and CNTs can facilitate charge transport to active sites, benefiting the electrocatalytic process. Otherwise, metal phthalocyanine (MPc) molecules could easily aggregate, and charge transport and electrocatalysis

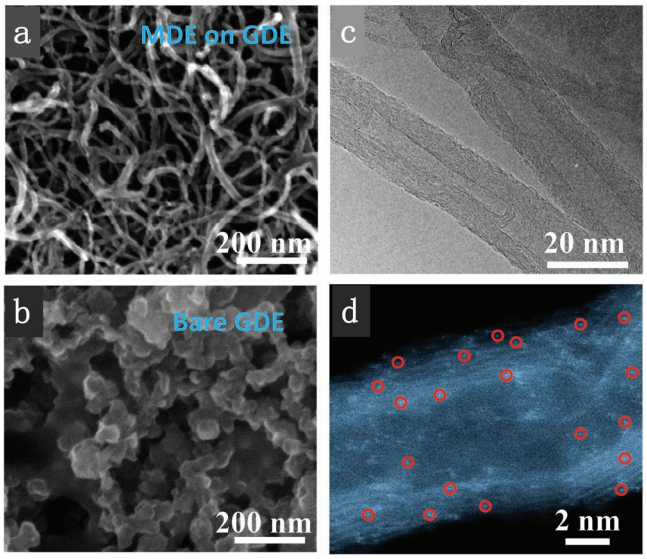

Figure 2. Morphology of NiPc-OMe MDE. The SEM images of a) NiPc-OMe MDE on GDE and b) bare GDE. c) Low magnification TEM image of NiPc-OMe MDE. d) HAADF-STEM image of NiPc-OMe MDE.

could be hindered due to their semiconducting nature.[33–36] The inductively coupled plasma mass spectrometry (ICP-MS) result suggests the presence of Ni in NiPc-OMe MDE, excluding the contamination of other metals (Table S1, Supporting Information). By tuning the ratio of molecules to CNTs, the Ni content was regulated to be ≈0.78 wt.%. The X-ray absorption near-edge structure (XANES) spectra at the nickel K-edge shows the electronic state of Ni in NiPc-OMe MDE is the same as that in pure NiPc-OMe (Figure S2, Supporting Information), suggesting the molecule maintains its original structure in MDE.

To investigate the electrocatalytic performance of CO_2RR in acid, the MDE samples were deposited on gas diffusion electrodes (GDEs). The scanning electron microscope (SEM) images show that NiPc-OMe MDE can uniformly cover the porous carbon layer of GDE (Figure S3, Supporting Information). The nanotube structure can be clearly observed and there are no large molecular aggregates (**Figure 2**a,b). The low magnification transmission electron microscope (TEM) image of NiPc-OMe MDE also shows a smooth surface of CNTs (Figure 2c), indicating the good dispersion state of NiPc-OMe in MDE. Z-contrast high-angle annular dark-field image of high-resolution aberration-corrected scanning transmission electron microscopy shows bright spots on the side walls of CNTs (Figure 2d), which correspond to the metal center of NiPc-OMe molecules, indicating the anchoring of NiPc-OMe on CNTs.

2.2. Selective CO_2RR in Acidic Electrolytes

Electrochemical performances were studied in a three-electrode flow cell system. 0.5 mol L^{-1} K_2SO_4 adjusted to pH 2 with H_2SO_4 was first used as the electrolyte, which was sufficiently acidic for CO_2 efficient utilization as reported.[26] Chronopotentiometry was conducted and product distributions at different current densities ranging from −20 to −400 mA cm^{-2} were analyzed (Figure S4, Supporting Information). It is surprisingly

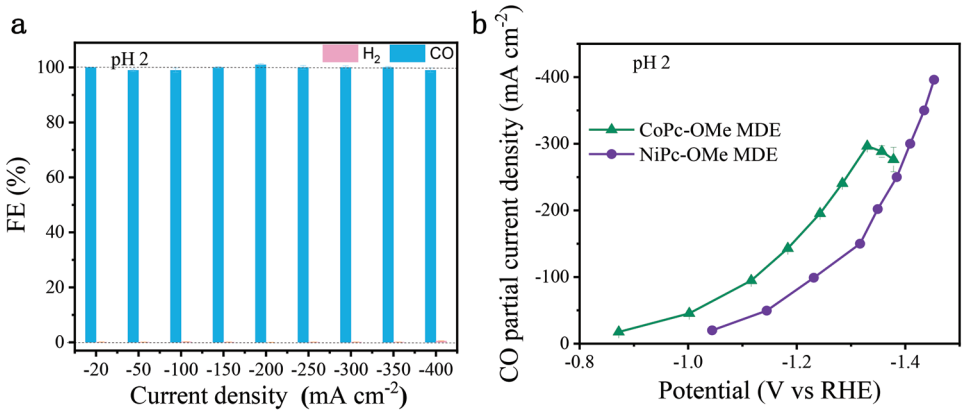

Figure 3. Acidic CO_2RR performances for NiPc-OMe MDE. a) FEs of CO and H_2 versus current density. b) CO partial current density as a function of applied electrode potential in H_2SO_4 adjusted 0.5 mol L^{-1} K_2SO_4 at pH 2.

found that NiPc-OMe MDE can effectively electrocatalyze CO_2RR to produce CO under this acidic condition (**Figure 3**a). The measured FE(CO)s are all >99%, indicating NiPc-OMe MDE can achieve nearly 100% electron utilization in acidic CO_2RR. This performance is better than the recently reported catalysts working at a similar acidic medium, such as the Au catalyst (FE(CO) 78% at −100 mA cm^{-2} in 1 mol L^{-1} Cs_2SO_4 with pH 2)[22] and Ni_5@NCN catalyst (FE(CO) 80% at −96 mA cm^{-2} in 0.25 mol L^{-1} Na_2SO_4 with pH 2.5).[20] More importantly, these reported catalysts can only guarantee their optimal selectivity in a narrow range of current densities, while the high selectivity of NiPc-OMe MDE is maintained in a wide range of current densities from −20 to −400 mA cm^{-2}. Consequently, NiPc-OMe MDE achieves high CO partial current densities of −396 mA cm^{-2} (Figure 3b), making it one of the best catalysts for CO production in acidic CO_2RR reported so far. Further, the CO_2RR performances of CNTs and NiPc-OMe were measured. As shown in Figure S5a,b (Supporting Information), CNT is not able to electrocatalyze CO_2RR, but pure NiPc-OMe can. However, the aggregated NiPc-OMe shows significantly lower FE(CO) (<30%) and larger overpotentials (>230 mV) than those of NiPc-OMe MDE (Figure S5b–d, Supporting Information), indicating the advantages of our MDE strategy for efficient CO_2RR.

We then examined the CO_2RR capability of the NiPc-OMe MDE under stronger acidic media (Figure S6, Supporting Information). Electrochemical tests were carried out in the K_2SO_4 solution with 0.05 mol L^{-1} (pH 1) or 0.1 mol L^{-1} H_2SO_4 (pH 0.47), respectively, and the cation (H^+ + K^+) concentration in the flowing electrolyte was tuned to be 1 mol L^{-1}. In the electrolyte of 0.05 mol L^{-1} H_2SO_4 + 0.45 mol L^{-1} K_2SO_4 (pH 1), NiPc-OMe MDE can still maintain its high CO production selectivity with FE(CO) >99% at the current densities ranging from −20 to −400 mA cm^{-2} (**Figure 4**a). In the electrolyte of 0.10 mol L^{-1} H_2SO_4 + 0.40 mol L^{-1} K_2SO_4 (pH 0.47), FE(CO) is only 66% at −20 mA cm^{-2} (Figure 4b), but rapidly increases to >98% as the current density increases beyond −50 mA cm^{-2}, and FE(CO) >99% can still be achieved at −100 mA cm^{-2} to −400 mA cm^{-2}. Although FE(CO) at pH 0.47 are slightly lower than those at higher pH, they are still much higher than the reported noble metal Au/C catalyst under the same strongly acidic condition,[19] where FE(CO) was only about 10% at −20 mA cm^{-2} and ≈70% at −50 mA cm^{-2}. The long-term operation of NiPc-OMe MDE was investigated at the current density of −100 mA cm^{-2} in 0.05 mol L^{-1} H_2SO_4 + 0.45 mol L^{-1} K_2SO_4 (Figure 4c). During 12 h of operation, the potentials maintain around −1.26 V with FE(CO) >99%, and almost no H_2 is detected during the whole process, indicating the good stability of NiPc-OMe MDE in acidic media.

2.3. The Role of K^+ in the Electrolyte

The effect of K^+ in the electrolyte was further studied. The CO_2RR of NiPc-OMe MDE was investigated in 0.1 mol L^{-1} H_2SO_4 electrolyte without any K_2SO_4 (**Figure 5**a). Unlike the presence of K^+ where FE(CO) is 98% at the current density of −50 mA cm^{-2}, almost no CO can be detected in 0.1 mol L^{-1} H_2SO_4 without K^+, and the measured FE(H_2) is 100%. With the current densities increased to −300 mA cm^{-2}, We could detect tiny CO products as the increase in current density could increase the local pH to favor CO_2RR. However, FE(CO)s are still below 1%, indicating the difficulty of CO_2RR in the absence of K^+ ions in strong acids for NiPc-OMe MDE. We further investigated the influence of K^+ concentration (Figure S7, Supporting Information). The H_2SO_4 concentration was kept at 0.1 mol L^{-1}, while the K_2SO_4 concentration varied from 0 to 0.1, 0.2, and 0.4 mol L^{-1}, respectively. The selectivity of CO gradually increases with the increase of K^+ concentration, while the corresponding H_2 by-products gradually decrease. Over 90% of FE(CO) could be achieved with ≥0.2 mol L^{-1} K_2SO_4. These results illustrate that the presence of sufficient K^+ is important for selective CO_2RR in acid.

We further compared the effect of K^+ on the HER of NiPc-OMe MDE by cyclic voltammetry (CV) in argon-protected 0.1 mol L^{-1} H_2SO_4 electrolyte and 0.1 mol L^{-1} H_2SO_4 + 0.4 mol L^{-1} K_2SO_4 electrolyte (Figure 5b; Figures S8 and S9, Supporting Information). The HER activity of NiPc-OMe MDE is substantially suppressed with K^+ presentation (Figure 5b). For example, it needs more than 500 mV overpotential to achieve HER current density of −50 mA cm^{-2} in the presence of K^+. Substantial reduction current is observed for NiPc-OMe below ≈−0.7 V in 0.1 mol L^{-1} H_2SO_4, which is attributed to the reduction of H^+.

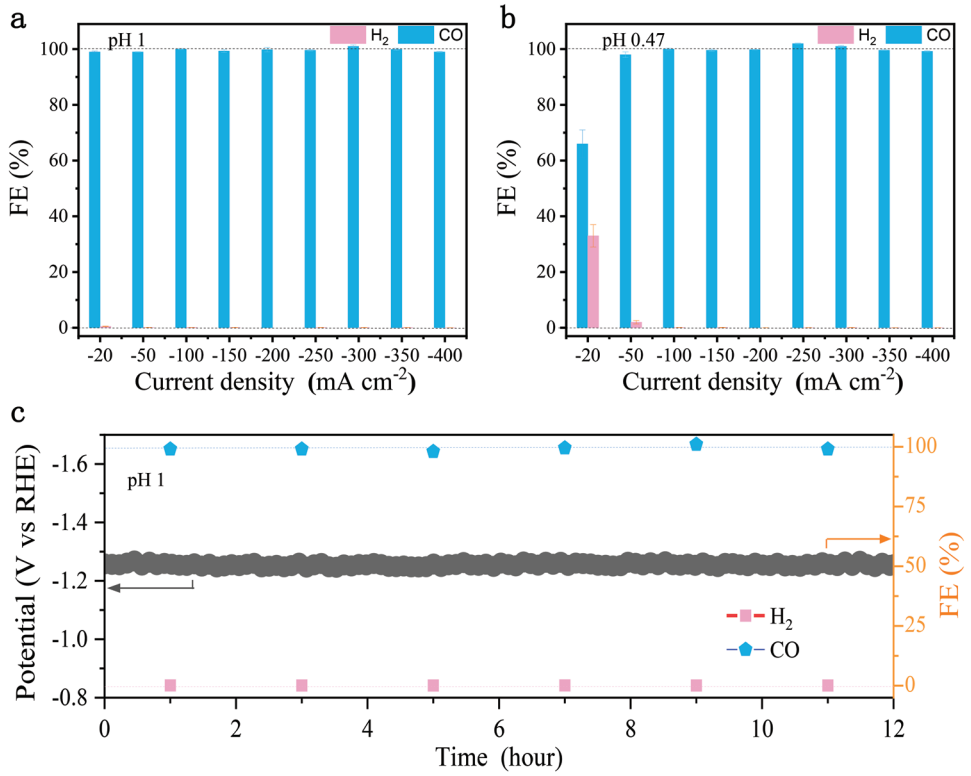

Figure 4. Electrocatalytic performances of NiPc-OMe MDE in stronger acidic media. FEs of CO and H_2 versus current density in a) 0.05 mol L^{-1} H_2SO_4 + 0.45 mol L^{-1} K_2SO_4 (pH 1) and b) 0.1 mol L^{-1} H_2SO_4 + 0.4 mol L^{-1} K_2SO_4 (pH 0.47). c) Chronopotentiometry and measured product FEs at the current density of –100 mA cm^{-2} for 12 h electrolysis.

In 0.1 mol L^{-1} H_2SO_4 + 0.4 mol L^{-1} K_2SO_4, two types of reduction current are observed below ≈–0.7 V: from ≈–0.7 to ≈–1.5 V, the reduction of H^+; below ≈–1.5 V, the reduction of water.[37] The H^+ reduction region becomes diffusion-limited with introducing of K^+, which can be verified by the rotating disk electrode study in Figure S8b (Supporting Information). As the H^+ concentration decreases with lower H_2SO_4 concentration, the current in the H^+ reduction region also becomes smaller (Figure S8a, Supporting Information). The above results suggest that the K^+ introduction in the electrolyte can reduce the H^+ concentration around the active site, because K^+ shields the electric field in the diffusion layer of the cathode.[19] Thus, HER is suppressed and CO_2RR can be performed on the active sites of NiPc-OMe MDE, leading to selective reduction of CO_2 to CO. However, this ability to suppress HER is partially offset by electrolytes with higher H^+ concentration, affording high FE(H_2) ≈33% for NiPc-OMe MDE at a low current density of –20 mA cm^{-2} at pH 0.47. Attributing to the rapid consumption of H^+ at higher current densities, the FE(H_2)s rapidly declined to <1% at the current densities larger than –100 mA cm^{-2} (Figure 4b).

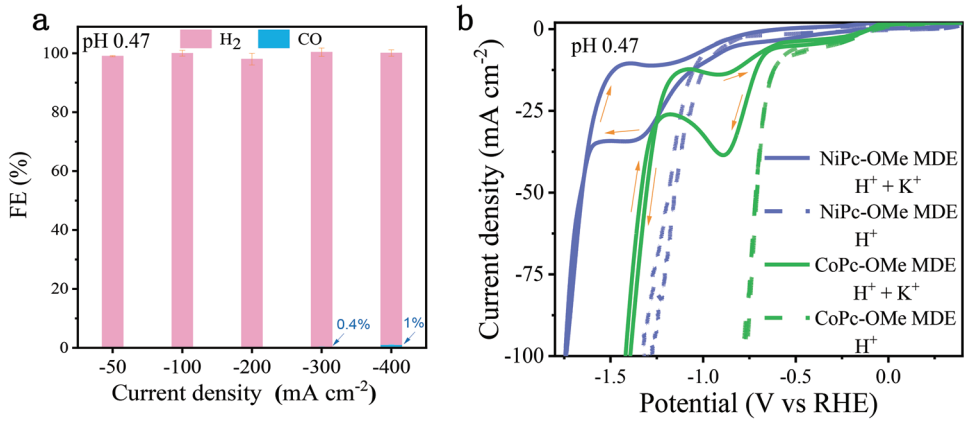

Figure 5. K^+ effect for the acidic CO_2RR of NiPc-OMe MDE. a) FEs of H_2 and CO for NiPc-OMe MDE in the 0.1 mol L^{-1} H_2SO_4 electrolyte. b) Cyclic voltammetry by NiPc-OMe MDE and CoPc-OMe MDE in argon-protected 0.1 mol L^{-1} H_2SO_4 or 0.1 mol L^{-1} H_2SO_4 + 0.4 mol L^{-1} K_2SO_4.

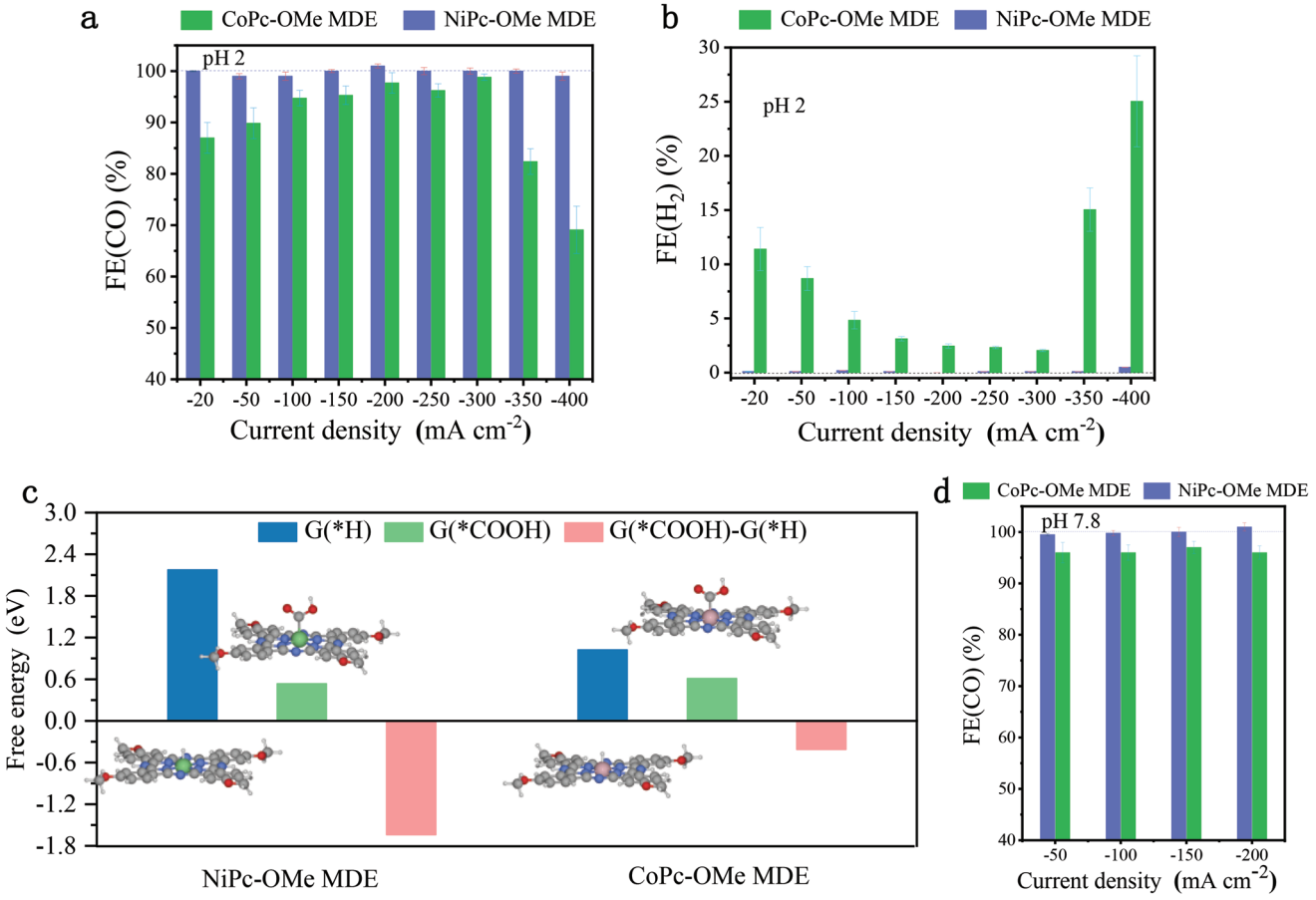

Figure 6. Electrocatalytic CO_2RR performance comparison between CoPc-OMe MDE and NiPc-OMe MDE. a) FE(CO)s and b) FE(H_2)s for NiPc-OMe MDE and CoPc-OMe MDE in 0.5 mol L^{-1} K_2SO_4 (pH 2, adjusted by H_2SO_4). c) The free energy for the formation of *COOH (G(*COOH)) or *H (G(*H)), and their energy difference (G(*COOH)–G(*H)) on NiPc-OMe and CoPc-OMe. d) FE(CO)s for NiPc-OMe MDE and CoPc-OMe MDE in 1 mol L^{-1} $KHCO_3$ (pH 7.8).

2.4. The Active Site Effect on High Selectivity in Acid

We then prepared CoPc-OMe MDE with a similar structure as NiPc-OMe MDE (Figure 1a) and tested it under the same conditions (Figure S10, Supporting Information). CoPc-OMe MDE shows a similar electrochemical active surface area (ECSA, Figure S11, Supporting Information) and charge transfer resistance (Figure S12, Supporting Information) as NiPc-OMe MDE. In 0.5 mol L^{-1} K_2SO_4 (pH 2, adjusted by H_2SO_4), CoPc-OMe MDE can also effectively eletrocatalyze CO_2RR to produce CO, indicating that the K^+ effect is also valid for CoPc-OMe MDE (**Figure 6**a,b). It is found that CoPc-OMe MDE exhibits higher electrocatalytic activity than NiPc-OMe MDE for CO_2RR (Figure 3b; Figure S13, Supporting Information), similar to the results reported in the neutral media.[38] But its FE(CO)s are inferior to NiPc-OMe MDEs at all tested current densities (Figure 6a). For example, FE(CO) is measured to be 87% at –20 mA cm^{-2}, and then gradually reached its maximum of 98% at –300 mA cm^{-2}. After that, FE(CO) turns into a sharp downtrend, and only 69% remains at –400 mA cm^{-2}. Consequently, its CO partial current density is limited to –296 mA cm^{-2}, 100 mA cm^{-2} lower than NiPc-OMe MDE (Figure 3b). This result also highlights the importance of high selectivity for CO production at high current densities to meet industrial production needs. The decline of FE(CO) is accompanied by the sharp increase of FE(H_2) (Figure 6b) and the initiation of methanol production (Figure S14, Supporting Information), which is consistent with our previous report that CoPc-based electrocatalysts can produce methanol at sufficiently negative potentials.[31] It should be noted that the CO selectivities of CoPc-OMe MDE are still superior to the reported electrocatalysts, such as Au,[19,22] Ag,[21] and Ni_5@NCN.[20]

The formation of adsorbed COOH and H intermediates on the active site (*COOH and *H) are considered to be the rate-determining step for CO_2RR and HER, respectively. We compared the free energy change difference for the formation of *COOH and *H (G(*COOH)–G(*H)) on NiPc-OMe and CoPc-OMe (Figure 6c). Although both NiPc-OMe and CoPc-OMe show a preference for CO_2RR, the much larger energy difference in NiPc-OMe can explain its higher FE(CO)s in acid (Figure 6c). It is also confirmed by HER performance comparison (Figure S15, Supporting Information), which shows that larger overpotentials were needed by NiPc-OMe MDE than CoPc-OMe MDE for operating at the same current densities. Noting that CoPc-OMe exhibits substantially lower CO selectivities in acid than in neutral conditions (Figure 6d). For

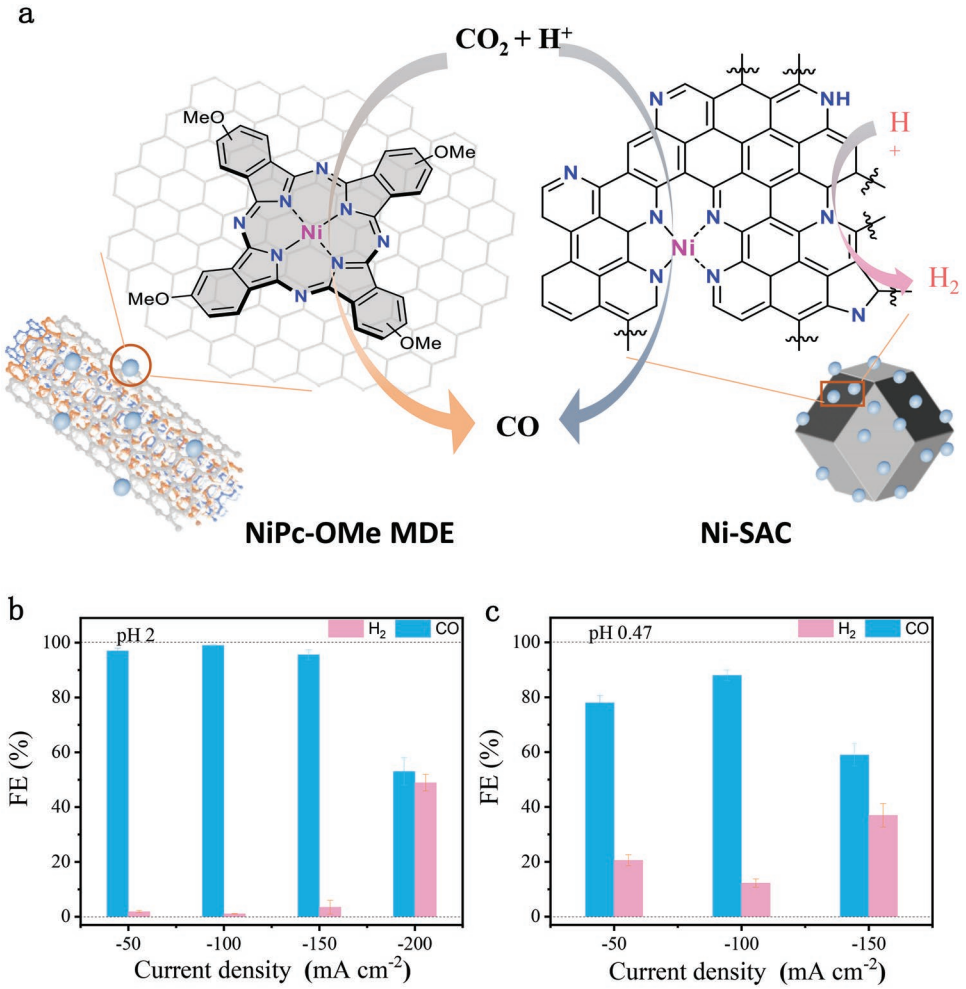

Figure 7. Electrocatalytic CO_2RR performance of Ni-SAC in acidic media. a) Schematic presentation of CO_2RR with NiPc-OMe MDE and Ni-SAC. FEs of CO and H_2 versus current density of Ni-SAC in b) 0.5 mol L^{-1} K_2SO_4 (pH 2, adjusted by H_2SO_4) and c) 0.1 mol L^{-1} H_2SO_4 + 0.4 mol L^{-1} K_2SO_4 (pH 0.47).

example, its FE(CO) can reach 96% at a current density of −50 mA cm^{-2} in neutral (1 mol L^{-1} $KHCO_3$, pH 7.8), but only 89% in acid. In sharp contrast, NiPc-OMe can well maintain its high FE(CO) even in acid. These results confirm the importance of the high selectivity of the active site for efficient acidic CO_2RR.

2.5. Comparison with Ni-SAC

We further investigated the acidic CO_2RR catalyzed by Ni-SAC with similar Ni-N_4 coordination active sites prepared by pyrolysis (**Figure 7**; Figure S16, Supporting Information).[39] In the electrolyte of pH 2, Ni-SAC could also exhibit high FE(CO)s of >95% at the current densities ranging from −50 to −150 mA cm^{-2} (Figure 7b). However, it fails to maintain high selectivities at higher current densities or in a stronger acidic medium (Figure 7b,c). The diverse structures generated by the high-temperature preparation process could account for these lower selectivities,[40–42] as HER can easily be activated at large overpotentials or in strongly acidic media on side reaction centers (Figure 7a). Therefore, the well-defined Ni-N_4 sites in NiPc-OMe MDE with little side reaction centers render it a more selective CO_2RR catalyst for CO production in acid.

3. Conclusion

In summary, we investigate the electrocatalytic performance of metal phthalocyanine-based MDEs for acidic CO_2RR and reveal that it can selectively produce CO in acid media with K^+. We show that K^+ in the electrolyte is beneficial to kinetically suppressing the HER, facilitating selective CO production of the molecular electrocatalysts. The intrinsic preference of CO_2RR over HER and none side reaction sites are also demonstrated important for high selectivity in acidic media for NiPc-OMe MDE. With these features, NiPc-OMe MDE shows highly selective CO_2RR with FE(CO) >98% over a wide range of current densities from −50 to −400 mA cm^{-2} under pH 2 to 0.47, achieving an unprecedented CO partial current density of −396 mA cm^{-2}. Our work demonstrates that NiPc-OMe MDE is a promising candidate for rapid and selective CO production in acidic CO_2RR. It also illustrates the advantages of molecular electrocatalysts for selective chemical conversion.

4. Experimental Section

Materials: All chemicals were purchased without further purification unless otherwise stated. *N*,*N*-dimethylformamide (DMF), potassium carbonate (K_2CO_3) and potassium sulfate (99%) were purchased from Aladdin. Concentrated sulfuric acid (H_2SO_4) (98%) and concentrated hydrochloric acid (35%) were purchased from Dongjiang Chemical Reagent. Multiwalled carbon nanotubes (CNTs, FT 9000) were purchased from C-Nano. And the CNTs were purified by calcining at 500 °C and washing with HCl (5 mol L^{-1}) solution as reported previously.[12,34] The Ni-SAC catalyst was prepared according to the reported method.[39] CO_2 (99.999%) and Ar (99.999%) were purchased from Huashidai Gas Co. Ltd. The gas diffusion layer (GDL, SGL29BC) and Ir/C (5%) were purchased from the Fuel Cell Store. Deionized water (18.2 MΩ cm) purified through a Pall water purification system was used throughout all experiments.

Electrode Preparation: The MDE sample (8.00 mg) was mixed in 3.6 mL Nafion solution (0.0325 wt.% in ethanol) and 0.4 mL PTFE solution (1%), and sonicated for 1 h to form MDE ink. 1.25 mL of the electrocatalysts ink was drop-dried onto a 1.0 × 2.5 cm^2 29BC CFP substrate (loading: 1.0 mg cm^{-2}). The working electrode was obtained by heating the catalyst-loaded carbon paper at 330 °C for 1 h under argon protection. The CNT electrodes without molecules were prepared in a similar way as NiPc-OMe MDE, except that MDEs were replaced with CNTs. Pure NiPc-OMe electrodes and Ni-SAC electrodes were prepared by dispersing NiPc-OMe or Ni-SAC in a Nafion ethanol solution (0.0325 wt.% in ethanol) with 2 mg mL^{-1}, and drop-dried on GDE with a loading of 1.0 mg cm^{-2}.

Electrochemical Methods: To investigate the electrocatalytic performance of CO_2RR in an acidic medium, the MDE samples were tested in a homemade three-electrode electrochemical flow cell with a gas diffusion electrode. The gas diffusion electrode can directly diffuse CO_2 to active sites and break the limitation of low CO_2 concentration in acidic electrolytes, which was beneficial to the CO_2RR performance of electrocatalysts. All electrochemical measurements were carried out with a CHI 660E potentiostat. The quadratic window for electrolysis was set to 0.5 × 1 cm^2, yielding an active area of 0.50 cm^2. Nafion 117 was used as the cation exchange membrane to separate the cathodic and anodic chambers. H_2SO_4(0.5 mol L^{-1}) was used as an anode electrolyte with a flow rate of 10 mL min^{-1}. The catholyte was argon saturated before flowing into the cathode with a flow rate of 6 mL min^{-2}. CO_2 was flowing at a rate of 30 mL min^{-1}. A 29BC substrate loaded with Ir/C (1.0 mg cm^{-2}) and an Ag/AgCl (filled with KCl solution) was used as the counter and reference electrodes, respectively. All potentials from the three-electrode experiments were converted to versus RHE with 80% *iR* correction by the following equation:

$$E_{RHE} = E_{Ag/AgCl} + 0.0591 \times pH + 0.210 - iR_u \quad (1)$$

The gas products were detected by online gas chromatography (GC9790Plus, FULI instrument) equipped with a flame ionization detector to quantify the CO fraction and a thermal conductivity detector to quantify the H_2 fraction. The calculation of gas phase products was based on measuring the actual flow rate of the gas outlet by a soap bubble flowmeter. Liquid products were quantified after electrocatalysis by ^{1}H NMR (Bruker 400-MHz NMR instrument).

Faraday efficiency (FE) of H_2, CO, and methanol were obtained by the following equation:

$$FE = \frac{ngxpF}{iRT} \quad (2)$$

The CO partial current density was obtained by the following equation:

$$\text{CO partial current density} = \frac{FE(CO)i}{S} \quad (3)$$

where *g* is the outlet flow rate, *x* is the fraction of H_2 or CO and methanol, *p* is 101 325 Pa, *F* is Faraday's constant (96487 C mol^{-1}), *i* is the operating current, *S* is a geometric area of the electrodes (0.5 cm^2), *n* is the numbers of electrons needed to generate one H_2, CO or methanol, *R* is the gas constant (8.314 J mol^{-1} K^{-1}) and *T* is 273.15 K.

Computational Methods: The free energy change to form adsorbed COOH and H intermediates on the metal phthalocyanine molecules in this study were performed using the Gaussian 09 program based on the reported method.[12]

Supporting Information

Supporting Information is available from the Wiley Online Library or from the author.

Acknowledgements

The authors acknowledge support from the National Natural Science Foundation of China (22075125), Guangdong-Hong Kong-Macao Joint Laboratory Fund (2019B121205001) and Shenzhen fundamental research funding (JCYJ20220818100618039, JCYJ20190809142415351). The authors sincerely thank Dr. Hua Zhou (Advanced Photon Source, Argonne National Laboratory) for his kind help in measuring X-ray absorption spectroscopy.

Conflict of Interest

The authors declare no conflict of interest.

Data Availability Statement

The data that support the findings of this study are available in the supplementary material of this article.;

Keywords

acidic electrolytes, CO_2 reduction, metal phthalocyanines, molecular electrocatalysis

Received: October 23, 2022
Revised: November 20, 2022
Published online:

[1] M. B. Ross, P. De Luna, Y. Li, C. Dinh, D. Kim, P. Yang, E. H. Sargent, *Nat. Catal.* **2019**, *2*, 648.
[2] P. De Luna, C. Hahn, D. Higgins, S. A. Jaffer, T. F. Jaramillo, E. H. Sargent, *Science* **2019**, *364*, eaav3506.
[3] H. Zhang, W. Cheng, D. Luan, X. W. Lou, *Angew. Chem., Int. Ed.* **2021**, *60*, 13177.
[4] P. Shao, W. Zhou, Q. L. Hong, L. Yi, L. Zheng, W. Wang, H. X. Zhang, H. Zhang, J. Zhang, *Angew. Chem., Int. Ed.* **2021**, *60*, 16687.
[5] S. Zuo, Z. Wu, H. Zhang, X. W. D. Lou, *Adv. Energy Mater.* **2022**, *12*, 2103383.
[6] D. Kim, S. Yu, F. Zheng, I. Roh, Y. Li, S. Louisia, Z. Qi, G. A. Somorjai, H. Frei, L.-W. Wang, P. Yang, *Nat. Energy* **2020**, *5*, 1032.
[7] M. Jouny, G. S. Hutchings, F. Jiao, *Nat. Catal.* **2019**, *2*, 1062.
[8] A. Ozden, Y. Wang, F. Li, M. Luo, J. Sisler, A. Thevenon, A. Rosas-Hernández, T. Burdyny, Y. Lum, H. Yadegari, T. Agapie, J. C. Peters, E. H. Sargent, D. Sinton, *Joule* **2021**, *5*, 706.

[9] M. Jouny, W. Luc, F. Jiao, *Nat. Catal.* **2018**, *1*, 748.
[10] T. Zheng, M. Zhang, L. Wu, S. Guo, X. Liu, J. Zhao, W. Xue, J. Li, C. Liu, X. Li, Q. Jiang, J. Bao, J. Zeng, T. Yu, C. Xia, *Nat. Catal.* **2022**, *5*, 388.
[11] H. Shin, K. U. Hansen, F. Jiao, *Nat. Sustain.* **2021**, *4*, 911.
[12] X. Zhang, Y. Wang, M. Gu, M. Wang, Z. Zhang, W. Pan, Z. Jiang, H. Zheng, M. Lucero, H. Wang, G. E. Sterbinsky, Q. Ma, Y. G. Wang, Z. Feng, J. Li, H. Dai, Y. Liang, *Nat. Energy* **2020**, *5*, 684.
[13] Q. Chang, Y. Liu, J.-H. Lee, D. Ologunagba, S. Hwang, Z. Xie, S. Kattel, J. H. Lee, J. G. Chen, *J. Am. Chem. Soc.* **2022**, *144*, 16131.
[14] M. Fang, L. Xu, H. Zhang, Y. Zhu, W. Wong, *J. Am. Chem. Soc.* **2022**, *144*, 15143.
[15] H. Guo, D.-H. Si, H.-J. Zhu, Q.-X. Li, Y.-B. Huang, R. Cao, *eScience* **2022**, *2*, 295.
[16] Z. Zhu, Z. Li, J. Wang, R. Li, H. Chen, Y. Li, J. S. Chen, R. Wu, Z. Wei, *eScience* **2022**, *2*, 445.
[17] M. Ma, E. L. Clark, K. T. Therkildsen, S. Dalsgaard, I. Chorkendorff, B. Seger, *Energy Environ. Sci.* **2020**, *13*, 977.
[18] S. Ren, D. Joulié, D. Salvatore, K. Torbensen, M. Wang, M. Robert, C. P. Berlinguette, *Science* **2019**, *365*, 367.
[19] J. Gu, S. Liu, W. Ni, W. Ren, S. Haussener, X. Hu, *Nat. Catal.* **2022**, *5*, 268.
[20] Z. Liu, T. Yan, H. Shi, H. Pan, Y. Cheng, P. Kang, *ACS Appl. Mater. Interfaces* **2022**, *14*, 7900.
[21] Z. Yan, J. L. Hitt, Z. Zeng, M. A. Hickner, T. E. Mallouk, *Nat. Chem.* **2021**, *13*, 33.
[22] M. C. O. Monteiro, M. F. Philips, K. J. P. Schouten, M. T. M. Koper, *Nat. Commun.* **2021**, *12*, 4943.
[23] J. E. Huang, F. Li, A. Ozden, A. Sedighian Rasouli, F. P. García de Arquer, S. Liu, S. Zhang, M. Luo, X. Wang, Y. Lum, Y. Xu, K. Bertens, R. K. Miao, C. T. Dinh, D. Sinton, E. H. Sargent, *Science* **2021**, *372*, 1074.
[24] C. J. Bondue, M. Graf, A. Goyal, M. T. M. Koper, *J. Am. Chem. Soc.* **2021**, *143*, 279.
[25] Y. Qiao, W. Lai, K. Huang, T. Yu, Q. Wang, L. Gao, Z. Yang, Z. Ma, T. Sun, M. Liu, C. Lian, H. Huang, *ACS Catal.* **2022**, *12*, 2357.
[26] Y. Xie, P. Ou, X. Wang, Z. Xu, Y. C. Li, Z. Wang, J. E. Huang, J. Wicks, C. McCallum, N. Wang, Y. Wang, T. Chen, B. T. W. Lo, D. Sinton, J. C. Yu, Y. Wang, E. H. Sargent, *Nat. Catal.* **2022**, *5*, 564.
[27] S. Lin, C. S. Diercks, Y.-B. Zhang, N. Kornienko, E. M. Nichols, Y. Zhao, A. R. Paris, D. Kim, P. Yang, O. M. Yaghi, C. J. Chang, *Science* **2015**, *349*, 1208.
[28] B. Zhang, L. Fan, R. B. Ambre, T. Liu, Q. Meng, B. J. J. Timmer, L. Sun, *Joule* **2020**, *4*, 1408.
[29] Y.-G. Wang, Z. Zhang, X. Zhang, Y. Yuan, Z. Jiang, H. Zheng, Y. G. Wang, H. Zhou, Y. Liang, *CCS Chem.* **2022**, *4*, 228.
[30] B. Siritanaratkul, M. Forster, F. Greenwell, P. K. Sharma, E. H. Yu, A. J. Cowan, *J. Am. Chem. Soc.* **2022**, *144*, 7551.
[31] Y. Wu, Z. Jiang, X. Lu, Y. Liang, H. Wang, *Nature* **2019**, *575*, 639.
[32] T. Yoshida, K. Kamato, M. Tsukamoto, T. Iida, D. Schlettwein, D. Whrle, M. Kaneko, *J. Electroanal. Chem.* **1995**, *385*, 209.
[33] Z. Jiang, Y. Wang, X. Zhang, H. Zheng, X. Wang, Y. Liang, *Nano Res.* **2019**, *12*, 2330.
[34] X. Zhang, Z. Wu, X. Zhang, L. Li, Y. Li, H. Xu, X. Li, X. Yu, Z. Zhang, Y. Liang, H. Wang, *Nat. Commun.* **2017**, *8*, 14675.
[35] M. Zhu, R. Ye, K. Jin, N. Lazouski, K. Manthiram, *ACS Energy Lett.* **2018**, *3*, 1381.
[36] J. Choi, P. Wagner, S. Gambhir, R. Jalili, D. R. Macfarlane, G. G. Wallace, D. L. Officer, *ACS Energy Lett.* **2019**, *4*, 666.
[37] J. Shen, R. Kortlever, R. Kas, Y. Y. Birdja, O. Diaz-Morales, Y. Kwon, I. Ledezma-Yanez, K. J. P. Schouten, G. Mul, M. T. M. Koper, *Nat. Commun.* **2015**, *6*, 8177.
[38] X. Zhang, Y. Wang, M. Gu, M. Wang, Z. Zhang, W. Pan, Z. Jiang, H. Zheng, M. Lucero, H. Wang, G. E. Sterbinsky, Q. Ma, Y. G. Wang, Z. Feng, J. Li, H. Dai, Y. Liang, *Nat. Energy* **2020**, *5*, 684.
[39] Y. Wang, Z. Jiang, X. Zhang, Z. Niu, Q. Zhou, X. Wang, H. Li, Z. Lin, H. Zheng, Y. Liang, *ACS Appl. Mater. Interfaces* **2020**, *12*, 33795.
[40] T. Möller, W. Ju, A. Bagger, X. Wang, F. Luo, T. Ngo Thanh, A. S. Varela, J. Rossmeisl, P. Strasser, *Energy Environ. Sci.* **2019**, *12*, 640.
[41] J. Zhang, W. Cai, F. X. Hu, H. Yang, B. Liu, *Chem. Sci.* **2021**, *12*, 6800.
[42] X. Wu, H. Zhang, S. Zuo, J. Dong, Y. Li, J. Zhang, Y. Han, *Nano-Micro Lett.* **2021**, *13*, 136.